Journal of Neuroscience Methods 182 (2009) 211–218

Contents lists available at ScienceDirect

Journal of Neuroscience Methods

journal homepage: www.elsevier.com/locate/jneumeth

Simple and cost-effective hardware and software for functional brain mapping using intrinsic optical signal imaging

Thomas C. Harrison[a,b], Albrecht Sigler[a,b], Timothy H. Murphy[a,b,c,d,*]

[a] Kinsmen Laboratory, Department of Psychiatry, 2255 Wesbrook Mall, University of British Columbia, Vancouver, BC, Canada V6T 1Z3
[b] Brain Research Center, 2255 Wesbrook Mall, University of British Columbia, Vancouver, BC, Canada V6T 1Z3
[c] Department of Cellular and Physiological Sciences, 2255 Wesbrook Mall, University of British Columbia, Vancouver, BC, Canada V6T 1Z3
[d] In Vivo Imaging Centre, 2255 Wesbrook Mall, University of British Columbia, Vancouver, BC, Canada V6T 1Z3

ARTICLE INFO

Article history:
Received 7 April 2009
Received in revised form 6 June 2009
Accepted 10 June 2009

Keywords:
In vivo imaging
Brain mapping
LED light sources
Sensory cortex
Mouse
Cranial surgery

ABSTRACT

We describe a simple and low-cost system for intrinsic optical signal (IOS) imaging using stable LED light sources, basic microscopes, and commonly available CCD cameras. IOS imaging measures activity-dependent changes in the light reflectance of brain tissue, and can be performed with a minimum of specialized equipment. Our system uses LED ring lights that can be mounted on standard microscope objectives or video lenses to provide a homogeneous and stable light source, with less than 0.003% fluctuation across images averaged from 40 trials. We describe the equipment and surgical techniques necessary for both acute and chronic mouse preparations, and provide software that can create maps of sensory representations from images captured by inexpensive 8-bit cameras or by 12-bit cameras. The IOS imaging system can be adapted to commercial upright microscopes or custom macroscopes, eliminating the need for dedicated equipment or complex optical paths. This method can be combined with parallel high resolution imaging techniques such as two-photon microscopy.

1. Introduction

Intrinsic optical signal (IOS) imaging was developed in the late 1980s to visualize activity-dependent changes in the reflectance of brain tissue and delineate functional areas (Grinvald et al., 1986). In the intervening years, IOS studies have contributed to our understanding of the olfactory bulb (Rubin and Katz, 1999) and the visual (Bonhoeffer and Grinvald, 1993; Grinvald et al., 1986), auditory (Bakin et al., 1996), and somatosensory (Masino et al., 1993) cortices. Because it is a simple technique compatible with *in vivo* imaging preparations, IOS is commonly used to target cortical areas for interventions such as stroke or microinjections, or to select areas for two-photon imaging (Brown et al., 2007; Schummers et al., 2008; Winship and Murphy, 2008). Although one could attempt to locate functional areas based on brain atlas coordinates, these can vary even between littermate mice. Furthermore, functional and anatomical relationships will change after interventions such as deafferentation (Pons et al., 1991) or stroke (Winship and Murphy, 2008), making it necessary to combine functional macroscopic imaging with studies of microscopic structure. We describe a system that is simple and inexpensive to construct and use, and provide details of small animal surgery to ensure successful preparations. It is our hope that this information will encourage more researchers to incorporate IOS into their *in vivo* experiments.

2. Methods

2.1. Objective-mounted LED ring lights

IOS has traditionally been performed using a tungsten halogen lamp coupled to a focusing lens, filter set, light guide, and shutter (Pouratian and Toga, 2002). Another possibility is to use light guides or through-lens LED illumination sources as employed for voltage-sensitive dye excitation or other forms of epifluorescence microscopy (Albeanu et al., 2008; Cescon et al., 2007; Nishimura et al., 2006). As a simpler alternative, we have devised an objective-mounted light-emitting diode (LED) light source. The low cost and small size of LEDs makes it possible to incorporate many lights into an unobtrusive ring light, which can be conveniently mounted to the objective lens (Fig. 1A and B). These LED ring lights produce spatially homogeneous light, and mounting to the objective automatically fixes their position relative to the focal plane. Because LEDs of appropriate wavelength for IOS are commercially available, no bandpass filters are required. A simple transistor circuit allows LEDs to be silently toggled on and off under electronic TTL control, eliminating the need for a mechanical shutter.

* Corresponding author at: Department of Psychiatry, University of British Columbia, 4N1-2255 Wesbrook Mall, Vancouver, BC, Canada V6T 1Z3.
Tel.: +1 604 822 0705; fax: +1 604 822 7981.
E-mail address: thmurphy@interchange.ubc.ca (T.H. Murphy).

0165-0270/$ – see front matter © 2009 Elsevier B.V. All rights reserved.
doi:10.1016/j.jneumeth.2009.06.021

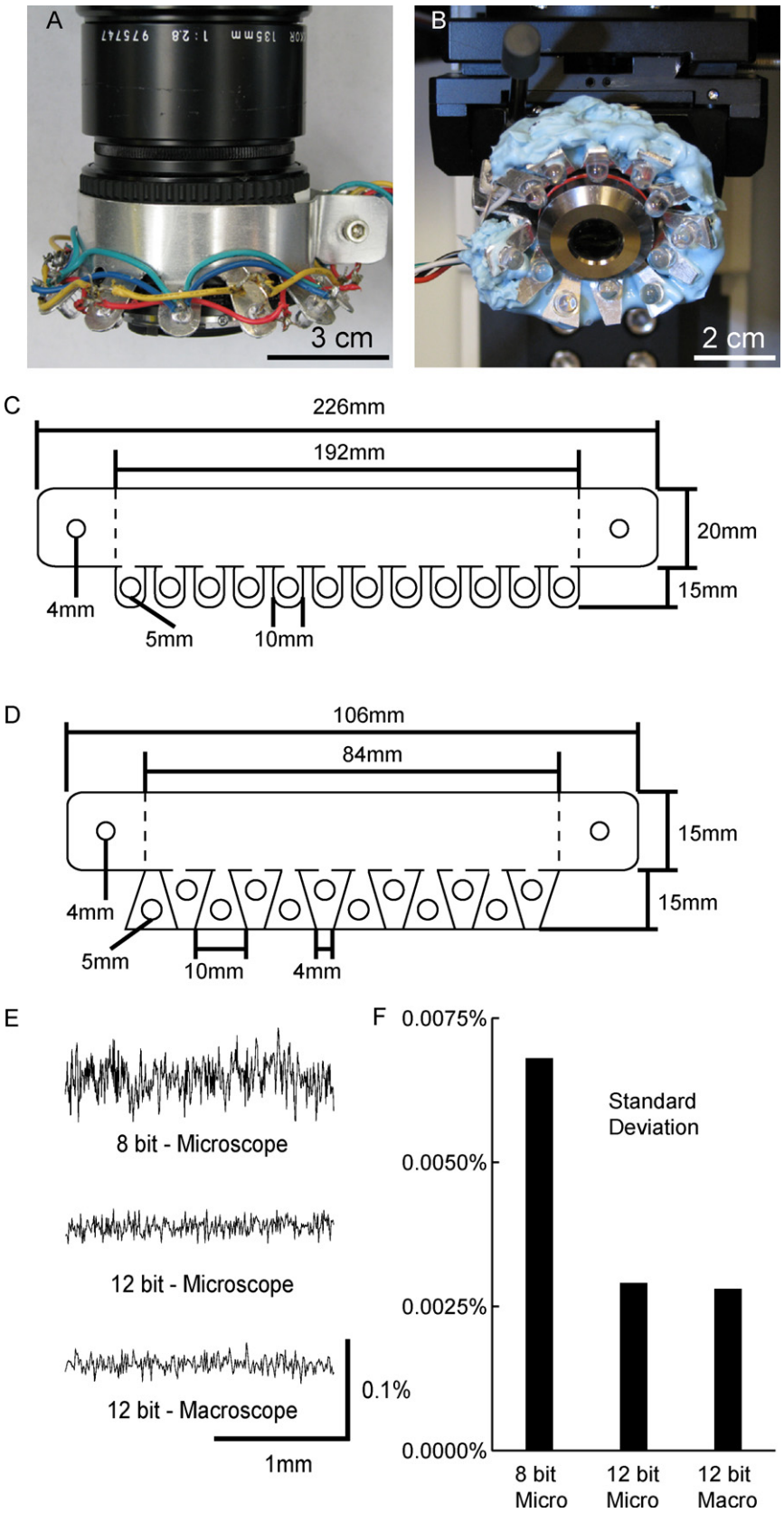

Fig. 1. LED ring lights. (A) Large ring light mounted to the objective of a macroscope. (B) Smaller ring lights fitted to a 4× microscope objective. Both rings hold 12 LEDs, with alternating red and green LEDs evenly spaced around the ring. (C and D) Dimensions of small (C) and large (D) rings. Dashes mark lines along which the 1 mm aluminum plate should be bent. (E) Noise plots of three IOS systems expressed as a percentage change from baseline. Imaging data from three IOS systems were collected using an inert test specimen and analyzed to give images representing percentage change in reflectance of 625 nm light. The percentage change was then determined across a 2 mm × 200 μm segment of each image to generate the noise plots (see Section 3). (F) Standard deviations of the three noise plots.

We construct ring lights from 1 mm-thick aluminum strips drilled to accommodate 5 mm-diameter through-hole mounted LEDs (Fig. 1C and D). IOS imaging can be performed with red LEDs only, but it is advantageous to have both green LEDs (525 nm, KSB1340-1P) for imaging brain vasculature at high contrast and red LEDs (625 nm, Knight Lites KSB1385-1P) to emphasize the rapid changes in blood oxygenation that accompany neuronal activity (Frostig et al., 1990). Wavelengths of light between 600 and 630 nm produce IOS maps with the greatest signal-to-noise ratio and spatial resolution (Pouratian and Toga, 2002). In this range of wavelengths, the decrease in reflectance associated with increased deoxyhemoglobin concentration lasts several seconds, and is followed by an increase in reflectance that can last up to 10 s as oxyhemoglobin concentration rise (Frostig et al., 1990). By restricting acquisition of response images to the first 1.5 s after stimulation onset, we predominantly detect the initial decrease in reflectance (Fig. 5D).

We have designed two ring sizes (Fig. 1C and D) for mounting either to macroscopes (Ratzlaff and Grinvald, 1991) or standard microscope objectives. The smaller ring (Fig. 1D) is used primarily with a 4×, 0.13 NA UPlan Fl Olympus objective 26 mm in diameter. The same ring light can also be attached to a 2.5×, 0.075 NA Plan Neofluar Zeiss objective, which is useful for maintaining a large field of view when using cameras with smaller CCD chips (e.g. Sony XC-ST70). The use of higher magnification objective lenses for functional mapping is not recommended because they limit both the field of view and the number of photons collected. In addition to the microscopes described above, we conduct IOS experiments using a macroscope constructed from front-to-front video lenses coupled with a 52 mm threaded adaptor ring (Nikon #4598). The top lens (closer to the camera) is a 135 mm F2.8 Nikkor and the bottom lens is a 50 mm F1.4 Nikkor manual focus lens (Nikon). Macroscopes are advantageous for IOS experiments due to their wide field of view (4.3 mm with Dalsa 1M60) and efficient light gathering. We also conduct IOS imaging using a combination of 50 and 35 mm lenses (top and bottom), which form a macroscope with a field of view of 8.2 mm (when used with a Dalsa 1M60 camera). This arrangement of lenses is useful for bilateral imaging experiments with mice or unilateral experiments with rats.

2.2. Powering the LED ring light

A stable power supply is the foundation of a good illumination system. Fluctuations of DC power will degrade IOS signals and preclude mapping even if power varies by as little as ~0.1% over tens of milliseconds. In many cases, standard laboratory constant-current power supplies are sufficiently stable for intrinsic optical signal imaging (e.g. Circuit-test PS-3330) (Fig. 1E and F). A large battery regulated with a potentiometer is also an ideal power supply. It is possible to use feedback-based systems employing photodiodes to ensure constant light output (Beach and Duling, 1993). In our hands, however, such devices only function well over a small range of currents and in some cases may produce more noise than they are designed to remove.

Ideally, power supplies should have a current limiting resistor in place to protect the LEDs from excessive current. If the LEDs are connected in parallel, the maximum allowable current is equal to the maximum current for a single LED multiplied by the total number of LEDs in the circuit. LEDs wired in series gain no such safety in numbers. If it is not possible to set a current limit on the power supply, a safety resistor should be added to the ring light circuit (Fig. 2A). The value of the resistor should be equal to the LED operating voltage divided by the maximum current, with an additional 10% added as a safety margin. For example, the red LEDs described above operate at 2.5 V with a maximum current of 0.1 A. If there are five LEDs wired in parallel, the maximum current is 0.5 A and so the safety resistor should have a value of 5 Ω plus an additional 10%. If the maximum voltage of the supply can exceed the operating voltage of the LEDs, the value of the resistor will need to be proportionally increased to protect the lights (e.g. a 50 Ω resistor should be used in the above circuit if it is powered by a 0–25 V supply).

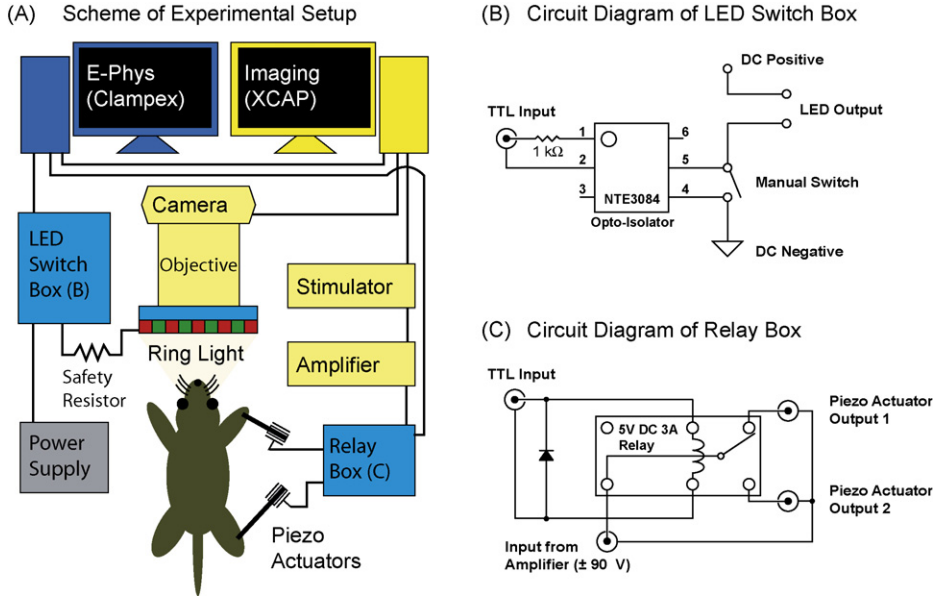

Fig. 2. Computer systems and circuitry for automated data collection. (A) Two computers are used to control the lights, camera, and somatosensory stimulators. One computer runs the electrophysiology program Clampex (Axon Instruments) and controls the timing of the ring light via a transistor-transistor logic (TTL)-controlled switch. This computer controls (via TTL) a second machine running XCAP (EPIX), which acquires imaging data from the camera and triggers the stimulator. (B) LED switch circuit for TTL control of LEDs. The LED switch incorporates an opto-isolator (NTE3084) to toggle the LEDs under TTL control and shield the LEDs from any electrical noise transmitted via the TTL lines. Manual switches can over-ride TTL control to activate the lights. When adjusting DC power levels to the LEDs, it is important to turn on the LEDs via TTL control and not with the manual switch, as these two circuits have different resistances and will result in different light levels. The connections from the DC power supply and the LED outputs are banana plugs, and the TTL connections are BNC-type. A safety resistor (A) should be placed between the LED switch box and the ring light to protect the LEDs (see Section 2). The relay box (C) receives amplified input from the stimulator and TTL input from the data acquisition computer, and transfers power to each piezo actuator alternately using a simple 5 V relay (Song Chuan 842-1C-C). All connectors are BNC-type. Both the LED switch and the relay circuits are housed in plastic casings.

2.3. Testing illumination stability

To assess the stability of illumination, we first determine the amount of LED light needed to fully illuminate the cortex. We operate our CCD cameras at approximately 80% of saturation (measured using EPIX XCAP image capture software), a value reached by adjusting the camera's exposure time and LED intensity. In general, signal-to-noise ratios improve with each additional photon collected. If light levels are insufficient to bring the CCD to 80% saturation (despite maximal exposure times and LED current), the ring light may require additional LEDs. We have found that with six of the red LEDs described and an exposure time of 100 ms, the camera can easily be brought to 80% saturation with sub-maximal LED current. Light levels should not exceed 90% of saturation anywhere in the image, as saturated pixels will degrade the IOS maps and render them useless.

Once the amount of light (LED current) necessary to bring the CCD camera to ~80% of capacity is established by adjusting brain illumination, one can begin experiments designed to check stability by collecting images in the absence of sensory stimulation or, better yet, by using an inert test specimen (Fig. 1E and F). Using the software provided in the supplementary materials, variation in baseline can be calculated by expressing signals as a percent change in light reflectance. If significant baseline variation is observed, e.g. a 0.05% variation in data integrated from 40 trials (see Section 3), one should optimize the illumination and/or detection systems. Using similar amounts of illumination light (measured with a power meter or photodiode, or estimated using the camera), different stabilized DC power sources can be evaluated. It may be necessary to employ a feedback system (Beach and Duling, 1993) to maintain a constant light level. It is important to optimize LED stability using a current level similar to that used to illuminate the brain because the variability of the power source and electronics is current-dependent. For a reflective non-biological test specimen we use a piece of polystyrene foam, altering reflectance (detected signal) to match that of the brain by covering the polystyrene with dark fabric or de-focusing. A flat and relatively homogeneous specimen such as a polystyrene foam block also allows one to adjust the position of LEDs for homogeneous illumination by bending individual tabs within the ring light, or by shifting the position of the entire unit on the objective lens. This should be done with the specimen in focus so that the lights are optimized for illumination of the focal plane. The microscope and sample should always be shielded from potentially varying ambient light by an opaque curtain during data acquisition.

2.4. Cameras and data acquisition

Stimulus-evoked intrinsic optical signals are relatively small changes in light reflectance, and even under optimal conditions tend to be less than one part in 400 (Grinvald et al., 1988). Given that 8-bit cameras can only measure one part in 255, it is not immediately clear how such a camera could be used to image these slight changes in signal. To allow detection of such small signals with relatively low-cost 8-bit cameras such as the Sony XC-ST70 (currently ~$900), the following steps are taken. First, a camera with a relatively high photon well capacity (such as the above-mentioned) should be chosen. Cameras with high well capacities are able to absorb more photons before saturating, improving signal-to-noise ratios by lowering Poisson noise (estimated by taking the square root of the number of photons collected) (Pawley, 2006). To increase sensitivity and ensure linearity, the infrared blocking filter should be removed from the chip face and automatic gain control disabled. To extend the 8-bit dynamic range we collect images at relatively high frame rates (30 Hz) and collapse across time to effectively boost well capacity. To increase signals further, we also integrate light from multiple stimulation trials and in space when regions of interest are used for calculations, and always perform calculations with 32-bit precision (see supplementary materials).

Although it is possible to perform IOS imaging with an 8-bit camera, greater bit depth is preferable. The camera we have the most experience with is the 12-bit Dalsa 1M60, which has a well capacity of 600,000 photons (Dalsa specifications). Compared with the Sony XC-ST70, the increased bit depth allows us to use lower frame rates (10 Hz) and reduce the total amount of data handled while still improving the signal-to-noise ratio. With the Dalsa 1M60 camera, we have found that a 10 Hz frame rate with 2×2 pixel binning is a good compromise between the number of photons collected and the size of image files. Given that IOS signals are slow, it would be possible to use frame rates lower than 10 Hz to reduce the amount of data collected. For example, one could take a single frame per second, using one pre-stimulation image as baseline and a second post-stimulation image as response. Such a procedure would work well for cameras with a very large photon well capacity, but with the Dalsa 1M60 camera this is disadvantageous since relatively fewer total photons can be collected. It is also important to point out that with the Dalsa 1M60, binning or integration will not change the total number of photons that can be collected per pixel. To collect the maximum number of photons from a specimen, one needs to increase frame rates and reduce binning (resulting in increased file size) since the number of photons collected per pixel is fixed. After images are acquired, analysis software can be used to bin or average floating point data to increase precision by sampling relatively larger numbers of photons.

Some practical considerations will apply to any camera. For example, lowering the focal plane to ~250 μm beneath the cortical surface helps to minimize biological noise from large surface blood vessels. If the curvature of the brain is very pronounced, it may be necessary to lower the focal plane further. A heat sink (e.g. Graftek AC-MS-0102) or active cooling device fitted to the Dalsa camera will also help to reduce noise by minimizing thermally generated pixels. However, these points are moot if excessive movement artifacts degrade the signal, so the animal should be held securely and the entire apparatus placed on a solid table. If a macroscope is used, mounting to an XYZ-translator (e.g. Sherline Tool #5430) facilitates both centering the sample (with respect to defined coordinates such as bregma) and focusing the image. The XYZ translator can be adapted for holding a camera by removing the tool mount and tapping the attachment point for 1/4″-20 mounting bolts.

It is common for researchers to use multiple computers to control the camera, deliver stimulation, and acquire data (Fig. 2A). For data acquisition, a frame grabber system must be capable of collecting image sequences at precise time intervals and reproducibly delivering an output signal. We currently use the EPIX frame grabber, but alternatives exist. Given variations in timing between different software packages, we find it best if the imaging software (EPIX XCAP) triggers the somatosensory stimulator directly (rather than another program). This will ensure that sensory stimulation is synchronized with image acquisition. Other parameters such as control of LED lights (Fig. 2B) or changing stimulation modalities (e.g. switching stimulation between fore- and hindlimbs, Fig. 2C) can be delegated to a second computer, as some degree of variation in timing is tolerable given that LED lights are switched on well before trials begin (>1 s). For a further check of synchrony between image acquisition and stimulation, we recommend mounting a red LED in place of the specimen and triggering it to coincide with stimulation. In this way an increase in LED signal will appear during stimulation and can be used to assess variation in synchronization between different trials. If one was concerned about synchronization during experiments, an LED pulse could be placed at the end of the trial to provide an internal standard for the entire time course of the experiment.

2.5. Surgical preparation

In our laboratory, we perform IOS imaging using three different types of animal preparations: the acute craniotomy, the chronic cranial window (Chen et al., 2004; Mostany and Portera-Cailliau, 2008), and the thinned skull preparation (Xu et al., 2007; Yoder and Kleinfeld, 2002). These procedures are approved by the University of British Columbia's animal care committee, in accordance with the guidelines of the Canadian Council on Animal Care. Detailed descriptions of surgical methods can be found in the supplementary materials.

IOS imaging will only be successful if the animal's head is held firmly in position, so we have designed a baseplate (Fig. 3A) to accommodate a Kopf Instruments Mouse Head Holder (model 926) on an adjustable arm fixed to the baseplate by a pivoting base (Thor Labs mounting hardware). The plate allows the mouse to be moved from the surgical area to the microscope stage, and is especially practical when the same animal is used for multiple experiments performed on different apparatuses (e.g. IOS and photothrombotic stroke). This freedom of movement allows the head to be tilted until the cortical surface is level. For experiments conducted under isoflurane anesthesia, a gas anesthesia mask (Kopf model 907) can be fitted to the head holder. When acute craniotomies are performed, the head holder is used in combination with a headplate (Fig. 3B) that is cemented to the skull to frame the craniotomy (Yoder and Kleinfeld, 2002). A well around the window holds agarose made in a saline solution, and a coverslip is cut to fit this well. The headplate can be bolted to two upright posts on the baseplate (Fig. 3C) (Grutzendler and Gan, 2006). For chronic cranial window and thinned skull preparations, the headplate is omitted in favor of ear bars (Kopf model 921).

2.6. Experimental design

Although any of the sensory cortices can be studied with IOS imaging, in our research we focus on the somatosensory cortex. Activation of the somatosensory cortex to elicit an IOS response can be achieved by stimulating various body parts, including the limbs, whiskers, tail, hips, shoulders, and trunk. For stimulation of the contralateral fore- and hindlimbs, we use an isolated pulse stimulator (AM Systems Model 2100) to drive two piezoelectric bending actuators (Piezo Systems Q220-AY-203YB) with a bi-phasic 4.5 V signal amplified to ±90 V by a high-voltage booster (Piezo Systems EPA-007-012) (Fig. 2A). Although the stimulator can produce a ±100 V signal, without the voltage booster it lacks sufficient current to properly drive the piezo. Each piezo is connected to one of the limbs by means of graphite pencil leads glued to the paw. A transistor-transistor logic (TTL)-controlled relay is used to alternate stimulation between the limbs (Fig. 2C). In these experiments, we delivered 1-s stimulus trains of 5 ms pulses at 100 Hz.

To reliably generate IOS maps, we perform up to 40 trials of stimulation per limb. It is usually possible to identify the activated areas with 10 trials, and after 20 trials the maps are generally well defined. Each trial begins by triggering the red lights and then collecting 15 baseline images at a frame rate of 10 Hz (Dalsa 1M60). One second of stimulation follows immediately after baseline acquisition, and 15 response images are collected during and after stimulation. Baseline and response images are compiled as multi-frame temporal stacks of TIFF files. Due to the slow time course of the hemodynamic response, we allow 20 s between stimulus trains to avoid any temporal overlap between trials.

2.7. Image analysis

Image analysis was conducted using a plugin for ImageJ (National Institutes of Health, Bethesda, MD; http://rsb.info.nih.gov/ij). The plugin, included as supplementary material and available in updated form online (neuroscience.ubc.ca/faculty/Murphy.html), creates IOS maps of cortical sensory representations based on IOS or voltage-sensitive dye (VSD) imaging data. The following analysis routine (Fig. 4) was performed using the ImageJ plugin described above: images were first converted to 32-bit depth to display results as decimals with high precision, and then the multi-frame image stacks were averaged across 40 trials. Next, we collapsed across time, averaging the 15 baseline and 15 response frames to a single frame each.

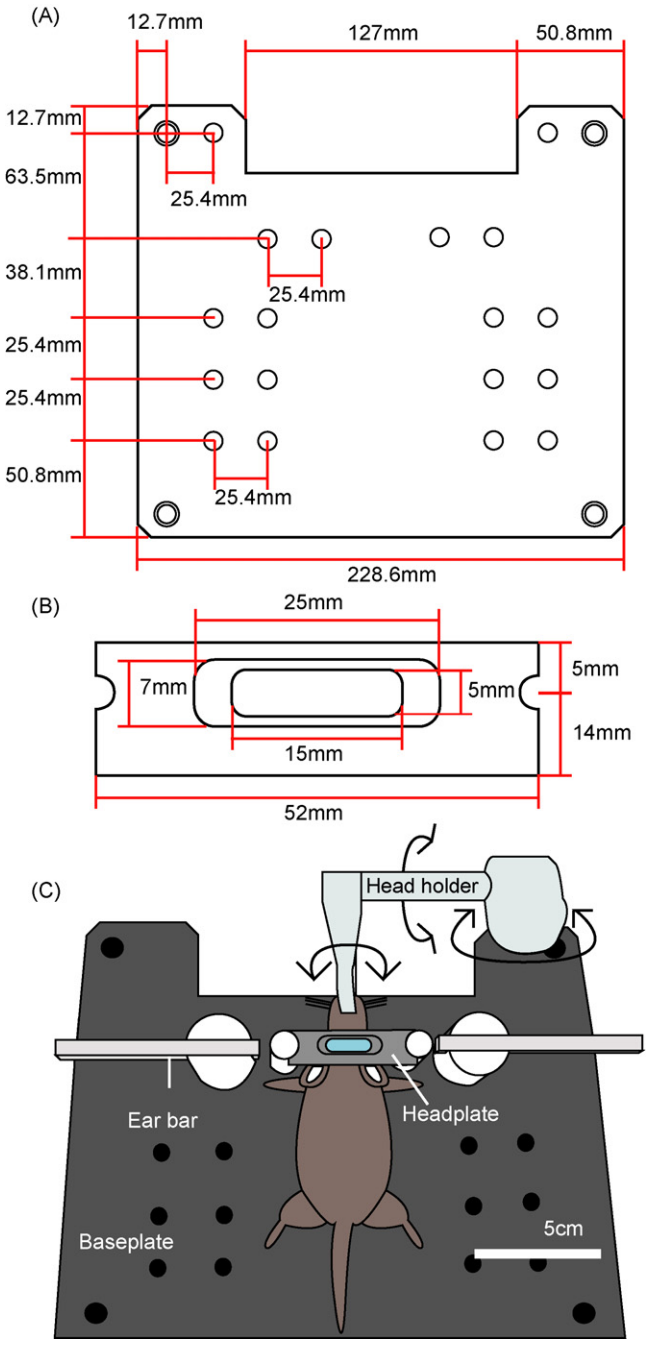

Fig. 3. Stereotactic apparatus for mechanically stable IOS imaging. (A) Baseplate designed to accommodate stereotaxic apparatus and mount to a microscope stage. The plate is made of 1 cm-thick anodized aluminum. (B) Headplate used to stabilize the preparation during acute experiments. (C) Diagram of mouse surgical preparation. The anesthetized mouse is placed on a feedback-controlled heating pad (not shown) on the baseplate. The mouse is then fitted with a stereotaxic head holder and either a headplate or earbars. The head holder is attached to the baseplate by an adjustable arm.

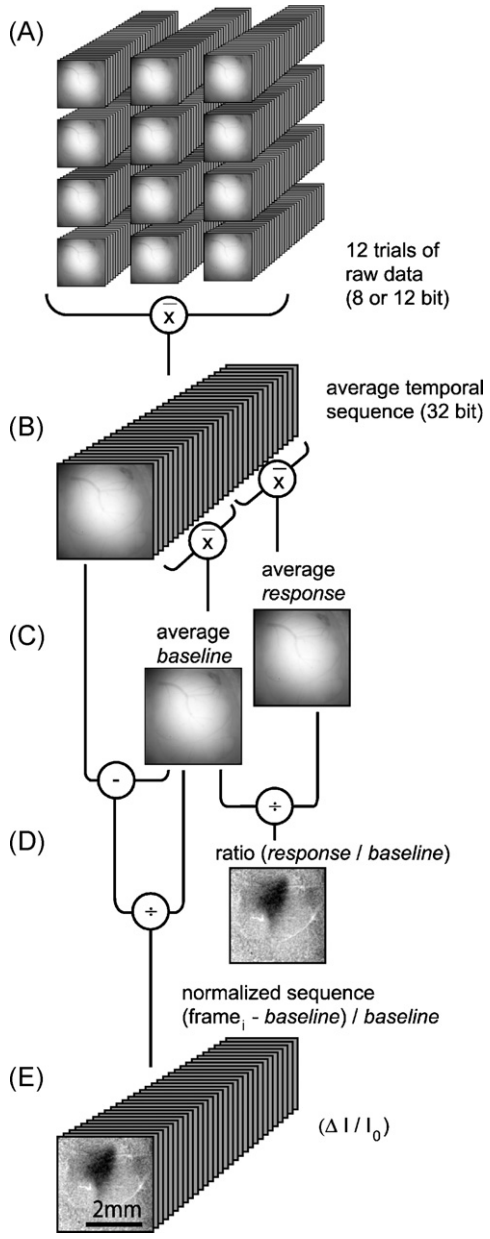

Fig. 4. Mathematical operations performed during IOS analysis. (A) Raw data are collected as temporal sequences of 30 sequential frames. (B) The image sequences are converted to 32-bit depth and then averaged across all trials. (C) The frames from the first half of the sequence, taken before stimulation, are averaged together to give a single baseline image. The average of the last half of the sequence, taken during and after stimulation, represents the response. (D) The ratio of the response and baseline can be calculated to generate a functional map. (E) To create a normalized video of changes in reflectance, each frame in the sequence has the baseline average subtracted from it and is then divided by the same baseline average. Scale bar applies to (B)–(E).

After Gaussian filtering against a kernel ($\sigma = 10\,\mu m$) in the *X* and *Y* dimensions, we compared baseline and response either by calculating their ratio or by dividing their difference by the baseline. As an additional step, each frame in the temporal sequence was normalized to the mean baseline image ($\%\Delta I/I_0$), yielding a video of percent changes in light reflectance over time.

3. Results

The ability to detect slight changes in reflectance is the key to successful IOS imaging, and requires consistent illumination. We characterized the temporal stability of our LED ring lights using a polystyrene test specimen as described in Section 2. This test was performed on three IOS systems used in our laboratory. System #1 incorporates a Sony XC-ST70 8-bit camera on an upright Olympus BX50WI microscope with a 2.5× objective. System #2 uses the same ring light (Fig. 1B) as system #1, but is fitted to a 4× objective on an Olympus BX51WI with a 12-bit Dalsa 1M60 camera. System #3 also uses a 12-bit Dalsa 1M60 camera, but images are captured through a macroscope and so a larger ring light is used (Fig. 1A). 40 trials were run on each system, and the data were analyzed using the same routine performed for IOS mapping. The percentage change between baseline and response was plotted for a region of interest of 2 mm in the *x*-dimension, averaged over 200 μm in the *y*-dimension. These plots (Fig. 1E) represent both the level of noise inherent to the system as well as spatial homogeneity across an image. To compare noise levels across the three systems, we calculated the standard deviations of the noise plots (Fig. 1F). For system #1 (Sony XC-ST70, 2.5× objective), this value was 0.0068%. System #2 (Dalsa 1M60, 4× objective) had a better noise profile (SD = 0.0029%), and system #3 (Dalsa 1M60, macroscope) was similar (SD = 0.0028%). After generating somatosensory maps (Fig. 5A–C), we performed a simple test to check for the presence of artifacts (see discussion on handling noisy data in the supplementary materials). Ideally, time plots of reflectance from regions of interest outside of sensory representations will show relatively constant reflectance over time, suggesting that changes within IOS maps are specific to somatosensory stimulation (Fig. 5D).

4. Discussion

4.1. Advantages of LED ring lights

Ring lights have several advantages over traditional illumination sources. By virtue of the spatial homogeneity of illumination they provide, LEDs represent an ideal light source for IOS. Even when 8-bit cameras are used to collect imaging data, the consistent illumination provided by LED ring lights permits good signal-to-noise ratios. When detecting such faint changes in reflectance, noise introduced by fluctuations inherent to arc or incandescent lamps can rapidly degrade the signal (Albeanu et al., 2008). Because they are fixed to the objective lens, LED ring lights maintain their position with respect to the objective focal plane, something that would be difficult to achieve with light guides. One alternative to light guides or ring lights would be to direct illumination light through the microscope objective. However, this requires an additional mirror and/or splitter, complicating the design and dividing the reflected light. Focusing light through the objective may also cause uneven illumination because the curvature of the brain results in a variable working distance. Ring lights work without the filter sets, shutters, and optics used in lamp-based illumination systems, simplifying the IOS system and reducing cost.

4.2. Combining IOS with two-photon microscopy

Two-photon microscopy is an excellent tool for investigating the fine structure of neurons, and can be combined with Ca^{2+} imaging *in vivo* to study cell function (Stosiek et al., 2003). This information is valuable, but needs to be placed in the context of the larger cortical areas in which these cells exist. IOS is a simple, non-invasive tool that can be used to delineate functional areas and guide higher-resolution investigations of cortical function. IOS can be combined with any form of sensory stimulation, permitting researchers to apply calcium indicators or other probes accurately in the sensory representation of interest (Brown et al., 2007; Schummers et al., 2008; Winship and Murphy, 2008; Zhang and Murphy, 2007).

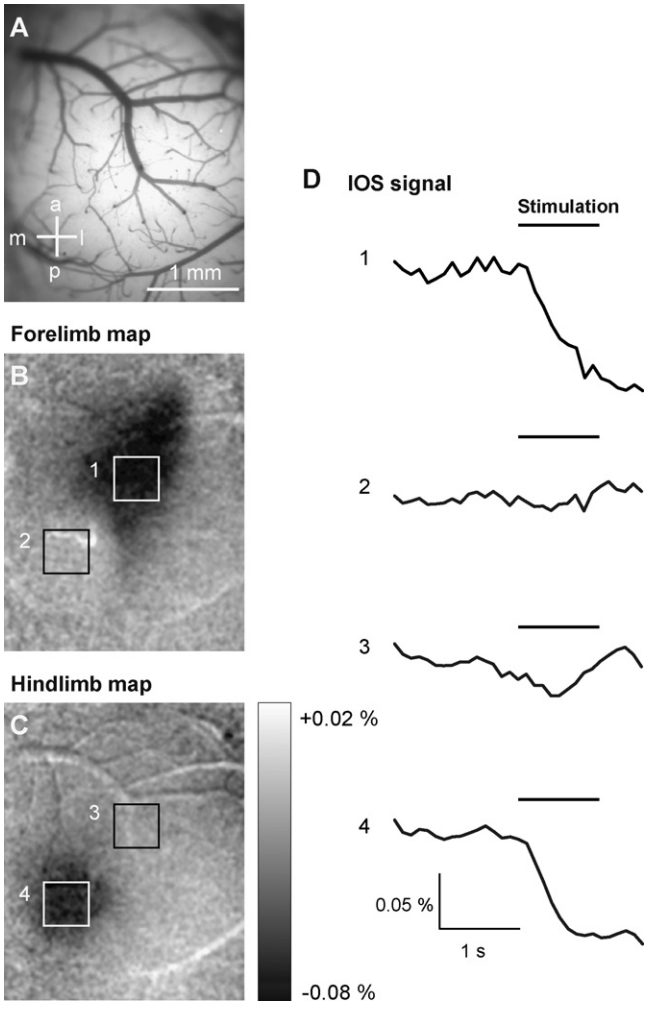

Fig. 5. IOS maps of mouse somatosensory representations. (A) The cortical surface illuminated with green light (525 nm). Anterior–posterior and medial–lateral directions are marked. Bregma is not marked, but the forelimb representation is located an average of 2.5 mm lateral and 0.5 mm anterior of bregma, with the hindlimb at 1.9 mm lateral and 0.6 mm posterior of bregma ($n = 5$ mice). (B) Forelimb and hindlimb (C) somatosensory maps of cortical area (A). Grey values are on a linear scale from a 0.02% increase in reflectance (white pixels) to a 0.08% decrease in reflectance (black). Scale bar in (A) also applies to (B) and (C). (D) Changes in reflectance of 625 nm light over time for the regions of interest numbered in (B) and (C). Regions 1 and 4, within the areas of activation, show a decrease in reflectance following somatosensory stimulation (marked with bar). Cortical regions outside of the somatosensory representations (2 and 3) show little change in reflectance after stimulation. The plots are the mean of 10 trials from a single animal, with a region of interest 0.07 mm^2.

The simplicity of our ring lights makes the IOS apparatus easy to incorporate into two-photon microscopes to permit low power IOS mapping in parallel with two-photon imaging of fine structure and function. IOS experiments require a CCD camera and the ability to produce a reflected light image of the brain. IOS imaging using ring lights is conducted without the use of excitation or emission filters, so a blank slot in the microscope's filter set is necessary. Most upright microscopes used for two-photon microscopy are already equipped with the hardware necessary to redirect the beam path from two-photon excitation/emission to a CCD camera, making it a simple process to accommodate both IOS and two-photon on the same microscope. For a description of the adaptations necessary to perform both CCD camera and two-photon imaging on a BX-51WI Olympus microscope see Sigler et al. (2008).

4.3. Variable illumination wavelength and spectroscopy

The wavelength of illumination will determine the physiological signal detected by IOS. We have used 625 nm LEDs to monitor rapid changes in blood oxygenation that accompanies neuronal activity (Frostig et al., 1990) and to optimize the spatial resolution of the resulting maps (Pouratian and Toga, 2002). Changes in total blood volume are best observed by illuminating the brain with 550 or 570 nm light, which is absorbed equally by oxy- and deoxyhemoglobin (Pouratian and Toga, 2002). Finally, longer wavelengths (>630 nm) can reveal activity-related light scattering believed to reflect cell-swelling and other blood-independent processes (Andrew and Macvicar, 1994; Cohen, 1973; Joshi and Andrew, 2001). One important observation is that all of these different response signals localize to the same cortical region, and therefore IOS maps will be very similar regardless of the imaging wavelength (Frostig et al., 1990).

Advances in optical design have made it possible to image the brain with multiple wavelengths of light simultaneously, allowing a three-dimensional representation of spectroscopic signals from living tissue to be constructed. This method, termed laminar optical tomography (LOT), detects functional changes in oxygenation levels in addition to providing structural information based on endogenous chromophores and fluorophores (Burgess et al., 2008). Multispectral reflectance imaging (MSRI), another extension of IOS involving multiple wavelengths of illuminating light, allows total hemoglobin concentration and blood oxygenation to be quantified (Dunn et al., 2003; Jones et al., 2008). Although LOT requires a complex optical system, ring lights could conceivably be adapted to incorporate LEDs of several different wavelengths in order to perform MSRI experiments. Spectral overlap between LEDs would be a limitation of ring lights however, and placing many different types of LEDs sparsely within the same ring light could also cause inhomogeneous illumination. These problems could likely be addressed with excitation filters, careful design of the ring lights, and possibly corrections performed in software.

Acknowledgements

This work was supported by operating grants to T.H.M. (MOP-12675) and the *In Vivo* Imaging Centre from the Canadian Institutes of Health Research. We acknowledge A. Goroshkov for design of the ring lights, and I. Drake and D. De Luca for their assistance with the circuit diagrams. We also thank P. Wang, H. Erb, and C. Jiang for surgical assistance.

Appendix A. Supplementary data

Supplementary data associated with this article can be found, in the online version, at doi:10.1016/j.jneumeth.2009.06.021.

References

Albeanu DF, Soucy E, Sato TF, Meister M, Murthy VN. LED arrays as cost effective and efficient light sources for widefield microscopy. PLoS One 2008;3:e2146.
Andrew RD, Macvicar BA. Imaging cell-volume changes and neuronal excitation in the hippocampal slice. Neuroscience 1994;62:371–83.
Bakin JS, Kwon MC, Masino SA, Weinberger NM, Frostig RD. Suprathreshold auditory cortex activation visualized by intrinsic signal optical imaging. Cereb Cortex 1996;6:120–30.
Beach JM, Duling BR. A light-emitting diode light standard for photo-microscopy and videomicroscopy. J Microsc (Oxf) 1993;172:41–8.
Bonhoeffer T, Grinvald A. The layout of iso-orientation domains in area 18 of cat visual cortex: optical imaging reveals a pinwheel-like organization. J Neurosci 1993;13:4157–80.
Brown CE, Li P, Boyd JD, Delaney KR, Murphy TH. Extensive turnover of dendritic spines and vascular remodeling in cortical tissues recovering from stroke. J Neurosci 2007;27:4101–9.

Burgess SA, Bouchard MB, Yuan BH, Hillman EMC. Simultaneous multiwavelength laminar optical tomography. Opt Lett 2008;33:2710–2.
Cescon C, Madeleine P, Graven-Nielsen T, Merletti R, Farina D. Two-dimensional spatial distribution of surface mechanomyographical response to single motor unit activity. J Neurosci Methods 2007;159:19–25.
Chen B, Trachtenberg JT, Holtmaat AJ, Svoboda K. Long-term, high-resolution imaging in the neocortex in vivo. In: Goldman RD, Spector DL, editors. Live cell imaging: a laboratory manual. Cold Spring Harbor: Cold Spring Harbor Laboratory Press; 2004. p. 423–34.
Cohen LB. Changes in neuron structure during action potential propagation and synaptic transmission. Physiol Rev 1973;53:373–418.
Dunn AK, Devor A, Bolay H, Andermann ML, Moskowitz MA, Dale AM, et al. Simultaneous imaging of total cerebral hemoglobin concentration, oxygenation, and blood flow during functional activation. Opt Lett 2003;28:28–30.
Frostig RD, Lieke EE, Tso DY, Grinvald A. Cortical functional architecture and local coupling between neuronal-activity and the microcirculation revealed by in vivo high-resolution optical imaging of intrinsic signals. Proc Natl Acad Sci USA 1990;87:6082–6.
Grinvald A, Frostig RD, Lieke E, Hildesheim R. Optical imaging of neuronal-activity. Physiol Rev 1988;68:1285–366.
Grinvald A, Lieke E, Frostig RD, Gilbert CD, Wiesel TN. Functional architecture of cortex revealed by optical imaging of intrinsic signals. Nature 1986;324:361–4.
Grutzendler J, Gan W-B. A practical guide: long-term two-photon transcranial imaging of synaptic structures in the living brain. In: Yuste R, Konnerth A, Masters BR, editors. Imaging in neuroscience and development: a laboratory manual. Cold Spring Harbor: Cold Spring Harbor Laboratory Press; 2006. p. 185–91.
Jones PB, Shin HK, Boas DA, Hyman BT, Moskowitz MA, Ayata C, et al. Simultaneous multispectral reflectance imaging and laser speckle flowmetry of cerebral blood flow and oxygen metabolism in focal cerebral ischemia. J Biomed Opt 2008:13.
Joshi I, Andrew RD. Imaging anoxic depolarization during ischemia-like conditions in the mouse hemi-brain slice. J Neurophysiol 2001;85:414–24.
Masino SA, Kwon MC, Dory Y, Frostig RD. Characterization of functional organization within rat barrel cortex using intrinsic signal optical imaging through a thinned skull. Proc Natl Acad Sci USA 1993;90:9998–10002.
Mostany R, Portera-Cailliau C. A craniotomy surgery procedure for chronic brain imaging. JoVE 2008:12.
Nishimura M, Shirasawa H, Song W-J. A light-emitting diode light source for imaging of neural activities with voltage-sensitive dyes. Neurosci Res 2006;54:230–4.
Pons TP, Garraghty PE, Ommaya AK, Kaas JH, Taub E, Mishkin M. Massive cortical reorganization after sensory deafferentation in adult macaques. Science 1991;252:1857–60.
Pouratian N, Toga AW.Toga AW, Mazziotta JC, editors. Brain mapping: the methods. New York: Academic Press; 2002.
Ratzlaff EH, Grinvald A. A tandem-lens epifluorescence macroscope—hundred-fold brightness advantage for wide-field imaging. J Neurosci Methods 1991;36:127–37.
Rubin BD, Katz LC. Optical imaging of odorant representations in the mammalian olfactory bulb. Neuron 1999;23:499–511.
Schummers J, Yu HB, Sur M. Tuned responses of astrocytes and their influence on hemodynamic signals in the visual cortex. Science 2008;320:1638–43.
Sigler A, Goroshkov A, Murphy TH. Hardware and methodology for targeting single brain arterioles for photothrombotic stroke on an upright microscope. J Neurosci Methods 2008;170:35–44.
Stosiek C, Garaschuk O, Holthoff K, Konnerth A. In vivo two-photon calcium imaging of neuronal networks. Proc Natl Acad Sci USA 2003;100:7319–24.
Winship IR, Murphy TH. In vivo calcium imaging reveals functional rewiring of single somatosensory neurons after stroke. J Neurosci 2008;28:6592–606.
Xu HT, Pan F, Yang G, Gan WB. Choice of cranial window type for in vivo imaging affects dendritic spine turnover in the cortex. Nat Neurosci 2007;10:549–51.
Yoder EJ, Kleinfeld D. Cortical imaging through the two-photon excitation laser intact mouse skull using scanning microscopy. Microsc Res Tech 2002;56:304–5.
Zhang SX, Murphy TH. Imaging the impact of cortical microcirculation on synaptic structure and sensory-evoked hemodynamic responses in vivo. PLoS Biol 2007;5:1152–67.